The influence of mesoscopic confinement on the dynamics of imidazolium-based room temperature ionic liquids in polyether sulfone membranes

Joseph E. Thomaz, Heather E. Bailey, and Michael D. Fayer[a)]
Department of Chemistry, Stanford University, Stanford, California 94305, USA

The structural dynamics of a series of 1-alkyl-3-methylimidazolium bis(trifluoromethylsulfonyl)imide ($C_n$mimNTf$_2$, n = 2, 4, 6, 10: ethyl—Emim; butyl—Bmim; hexyl—Hmim; decyl—Dmim) room temperature ionic liquids confined in the pores of polyether sulfone (PES 200) membranes with an average pore size of ~350 nm and in the bulk liquids were studied. Time correlated single photon counting measurements of the fluorescence of the fluorophore coumarin 153 (C153) were used to observe the time-dependent Stokes shift (solvation dynamics). The solvation dynamics of C153 in the ionic liquids are multiexponential decays. The multiexponential functional form of the decays was confirmed as the slowest decay component of each bulk liquid matches the slowest component of the liquid dynamics measured by optical heterodyne-detected optical Kerr effect (OHD-OKE) experiments, which is single exponential. The fact that the slowest component of the Stokes shift matches the OHD-OKE data in all four liquids identifies this component of the solvation dynamics as arising from the complete structural randomization of the liquids. Although the pores in the PES membranes are large, confinement on the mesoscopic length scale results in substantial slowing of the dynamics, a factor of ~4, for EmimNTf$_2$, with the effect decreasing as the chain length increases. By DmimNTf$_2$, the dynamics are virtually indistinguishable from those in the bulk liquid. The rotation relaxation of C153 in the four bulk liquids was also measured and showed strong coupling between the C153 probe and its environment. *Published by AIP Publishing.* https://doi.org/10.1063/1.5003036

I. INTRODUCTION

Room temperature ionic liquids (RTILs) are an emergent class of important solvents with potential applications in a wide variety of fields. These compounds are classified as molten salts and as such remain liquids at room temperature. They are typically characterized by a large asymmetric organic cation with a poorly coordinating more inorganic anion. The wide variety of potential cations and anions that result in RTIL formation makes it possible to select the combination to optimize desired properties such as negligible vapor pressure,[1] low flammability,[2] thermal stability,[3] and high solubility of CO_2.[4,5]

An important attribute of ionic liquids, which has attracted considerable interest, is their ability to form nanodomains that involve the segregation of local ionic and apolar regions.[6–8] Since nanodomains' formation was first noticed via molecular dynamics simulations,[6–8] the picture of segregation has been used to explain a variety of experimental data in X-ray scattering,[9,10] dielectric spectroscopy,[11,12] neutron magnetic resonance (NMR) spectroscopy,[10,13,14] fluorescence spectroscopy,[15–17] optical heterodyne-detected optical Kerr effect (OHD-OKE) experiments,[18–20] and two-dimensional infrared (2D IR) spectroscopy.[21,22] It is important to clarify that not all RTILs have the capability of forming these nanodomains. For instance, in the case of imidazolium-based RTILs,

calculations demonstrated that the positive charge on the imidazolium cation is delocalized over the first two carbons of any alkyl chain moiety;[8] apolar regions only form in compounds containing an alkyl chain with four or more carbons on the cation, which has been verified by experiments.[10–21] Furthermore, it was determined that clear nanodomains were not present until the alkyl chain reached a length of six carbons.[14,23–25] In the study presented here, a series of 1-alkyl-3-methylimidazolium bis(trifluoromethylsulfonyl)imide RTILs where alkyl is 2, 4, 6, and 10[26] carbons (Emim, Bmim, Hmim, and Dmim) were used to span the range from liquids that have no apolar regions to those with substantial apolar regions. The structure of these RTILs is given in Fig. 1(a).

Membrane sciences have generated a considerable amount of interest in the field of separations, particularly supported liquid membranes (SLMs).[14] Their ability to provide a high degree of selectivity while consuming considerably less solvent than alternative separation methods has made them desirable for applications in industry as they limit the amount of chemical pollutants released into the atmosphere.[27] RTILs are also very useful solvents in the field of separations, demonstrating a high ability for selectivity in capturing CO_2 molecules.[4,28,29] Ionic liquids in porous membranes are referred to as supported ionic liquid membranes (SILMs) and have emerged as an active area of study.[26,30,31] The low volatility of the RTIL results in an even lower solvent loss than conventional solvents, and the RTIL stabilizes the membrane more effectively.[26] Figure 1(b) gives the structure of a polyether sulfone (PES) monomer unit, a polymer used to make

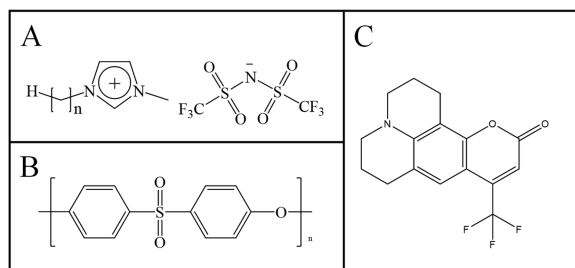---

a)Email: fayer@stanford.edu. Telephone: 650 723-4446.

FIG. 1. Chemical structures of (a) 1-alkyl-3-methylimidazolium bis(trifluoromethylsulfonyl)imide, (b) polyether sulfone monomer unit, (c) coumarin 153.

nanoporous membranes that are commonly employed as SILMs.

Recently, there have been a number of studies of RTILs near interfaces that indicate that the influence of an interface on the RTIL structure persists for a significant distance into the liquid.[32,33] Studies of an ionic liquid in PES SILMs have shown that the dynamics of the RTIL, EmimNTf$_2$ (1-ethyl-3-methylimidazolium bis(trifluoromethylsulfonyl)imide), slow substantially when confined in the PES membrane pores.[32,33] The surprising aspect of these studies is that the pores were very large, on average 350 nm in diameter in PES 200. The liquid dynamics, which are a reflection of liquid structure, are significantly influenced by confinement in such large pores which is remarkable as it differs from the behavior of other liquids in confinement. For example, water in AOT reverse micelles displays bulk-like behavior away from the immediate vicinity of the interface once the diameter of the water pool is greater than ~6 nm.[34] Therefore, there is evidence that RTILs behave in a fundamentally different manner in confined environments than other liquids. The interface has a much longer range influence on dynamics and structure. In experiments conducted using ultrafast infrared techniques on vibrational probes in EmimNTf$_2$ confined in the pores of the SILMs, the examination of dynamics was limited to this one RTIL and relatively short time scales, ~100 ps. Thus the influence of confinement on RTILs with different alkyl chain lengths and on the full range of the RTILs' dynamical time scales was not addressed.

Here we present time-dependent fluorescence Stokes shift experiments that measure solvation dynamics using a fluorescent probe molecule[35–38] in a series of C$_n$mimNTf$_2$ RTILs in the bulk liquid form and confined as PES 200 SILMs. Because of the long lifetime of the fluorescent probe, it was possible to study the full range of dynamics in the liquids. The technique has been employed extensively to measure the bulk dynamics of a variety of solvents.[35–38] In this method, a molecular probe is selected such that, upon excitation, a significant change in the dipole moment in the excited state induces the surrounding solvent to reorganize to compensate for the change in dipole. This inherently nonequilibrium process is subject to Onsager's regression hypothesis (linear response theory) which states that the solvent relaxation occurs through equilibrium solvent fluctuations. In the experiments,[39] the liquid response is obtained by measuring the time-dependent shift of the fluorescence emission maximum (Stokes shift) until the solvent has completely relaxed to accommodate the dipole moment

change when the chromophore is excited. The process is illustrated in Fig. 2. Immediately after excitation, the fluorescence is centered at $\nu(t = 0)$. As the solvent reorganizes, the emission center of the fluorescence moves until it ceases to shift at $\nu(t = \infty)$ because the solvent has reached its new equilibrium configuration.[40,41] In ionic liquids, the Stokes shift is relatively slow, extending well into the nanosecond regime.[35,40,42–44]

In the experiments presented below, the fluorescence probe is coumarin 153 [C153, see Fig. 1(c)], which is used to study the dynamics of the RTILs as bulk liquids and confined liquids in PES 200 membranes. Detailed measurements to determine the location of aromatic compounds within alkylimidazolium-based RTIL solutions have shown that compounds containing few aromatic rings lie in the ionic region of RTILs as a result of π-stacking interactions.[45,46] In contrast, this was not found to be true in larger polyaromatic compounds.[46] C153 contains only two aromatic rings and is therefore expected to locate in the ionic regions of the RTILs. Simulations by Terranova and Corcelli indicate that this is the case for C153.[47]

Optical heterodyne-detected optical Kerr effect (OHD-OKE) experiments were also conducted to study the orientational dynamics of the bulk RTILs. For complex systems of large ions, such as the RTILs studied, complete orientational relaxation will not occur without total randomization of the liquid structure. This method is uniquely suited for bulk studies because it is a nonresonant experiment that requires no addition of a resonant probe and is not lifetime limited. OHD-OKE experiments have previously been used to study a wide range of liquids including ionic liquids,[48,49] liquid crystals,[50,51] and supercooled liquids.[52,53]

In the experiments presented below, the time-dependent Stokes shift measurements are compared to the OHD-OKE measurements for the bulk RTILs. It was found that the slowest decay component of the Stokes shift matches the slowest exponential decay component of the OHD-OKE data in all four liquids. This identifies the slowest component of the Stokes shift as the time for complete structural randomization of the liquid. It also confirms that the Stokes shift data is a multiexponential decay rather than a stretched exponential, which is frequently used to model Stokes shift data. Although the pores in the PES membranes are large (~350 nm), confinement on
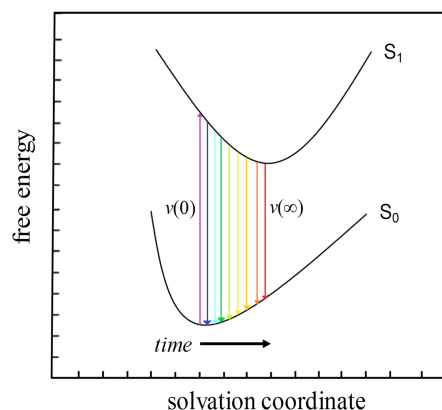

FIG. 2. A schematic illustration of the time-dependent Stokes shift (exaggerated for clarity). As time progresses, the fluorescence emission wavelength shifts to the red (lower frequency).

the mesoscopic length scale results in substantial slowing of the dynamics, a factor of ~4 for EmimNTf$_2$, with the effect decreasing as the chain length increases. By DmimNTf$_2$, the dynamics are virtually indistinguishable from those in the bulk liquid. The slowest component of the Stokes shift decays in the SILMs is identified as the time for complete structural randomization of the RTILs in the pores in analogy to the results obtained for the bulk liquids. Thus, confinement has a major influence on the RTIL structural relaxation in the membrane for EminNTf$_2$, and the influence of confinement decreases as the alkyl chain length increases.

II. MATERIALS AND METHODS

C$_n$mimNTf$_2$ ionic liquids were ordered from IoLiTec at 99% high purity (HP) grade and were subsequently placed in vacuum and dried for one week at a temperature of 60 °C. It was determined through Karl Fischer titration that the water content was below 30 ppm. Due to their hygroscopic nature, the ionic liquids were then stored in a glovebox, and all further sample preparations were conducted in a glovebox. It has been shown that changes in ionic liquid properties are negligible for water contents less than 100 ppm.[54] For Optical Heterodyne-Detected Optical Kerr Effect (OHD-OKE) experiments, samples were filtered using a 0.02 μm filter (Whatman Anotop) into a 1 cm optical grade cuvette. All fluorescence and OHD-OKE experiments were performed in the same room at an ambient temperature of 297.5 K.

C153 was purchased from TCI America at 98% purity. Samples for the fluorescence experiments were prepared such that the final concentration of C153 in the ionic liquid was 10^{-4}M. For fluorescence experiments, bulk C$_n$mimNTf$_2$ solutions were injected into a 1 mm path length cuvette, which were stoppered and parafilmed. PES 200 polyether sulfone membranes (Supor® 200) were purchased from the Pall Corporation. These membranes were immersed in a C$_n$mimNTf$_2$ ionic liquid stock solution containing C153 for 3 h. They were wiped such that no ionic liquid remained on the membrane surface. The membranes were placed in a 1 cm path length cuvette, stoppered, and further sealed with parafilm. Ionic liquids frequently have some fluorescent emission from a small amount of contamination.[55] Due to high purity of the ionic liquids, the background fluorescence of the samples was determined to be three orders of magnitude lower than that of the C153 probe, resulting in a negligible contribution to the emission signals.

Fluorescence solvation dynamics experiments were conducted utilizing time correlated single photon counting (TCSPC). A Ti:sapphire oscillator producing approximately 100 fs laser pulses at an excitation wavelength of 790 nm was employed. This wavelength was frequency doubled in a barium borate crystal to 395 nm for excitation of C153. The bandwidth of the 395 nm excitation pulse was 5.8 nm. The laser repetition rate was lowered from 80 MHz to 5 MHz by means of an acousto-optic modulator functioning as a single pulse selector. A computer-controlled half waveplate rotated the excitation beam such that measurements could be collected parallel, perpendicular, and at a magic angle relative to a fixed polarizer secured at the entrance slit of a monochromator. The sample was excited from the front surface in a near-normal geometry

through a hole in the lens that collected the fluorescence. A second lens imaged the fluorescence onto the monochromator entrance slit. The fluorescence was frequency resolved by the monochromator, and single photons were detected with a multichannel plate (MCP) detector at wavelengths ranging from 460 nm to 580 nm.

The instrument response was obtained by measuring the fluorescence lifetime of aqueous acidified malachite green with an optical density matching that of the sample, under identical experimental conditions to the sample measurements. Malachite green has an extremely short fluorescence lifetime, 5 ps,[56] which is short compared to the instrument response. Measurement of its fluorescence lifetime on this system gives the instrument response including the effects of the finite thickness of the sample cell. The instrument response was no greater than 70 ps.

Solvation dynamics measurements were made with the excitation polarization set to the magic angle. Population decay curves were then collected from 460 nm to 580 nm in 2 nm increments. Each emission wavelength was collected for 60 s. The wavelength scan was repeated until it was determined that an acceptable signal-to-noise level had been reached. All data were taken with the same entrance slit width, and all other experimental conditions were identical so that the relative amplitude at each emission wavelength was correct. Fluorescence orientational relaxation measurements of C153 are discussed in the supplementary material.

OHD-OKE experiments were conducted to measure the orientational dynamics of the bulk liquid. The OHD-OKE experimental setup has been described in detail previously,[20,48] but a short summary is given here. An 86 MHz Ti:sapphire oscillator generates pulses centered at 800 nm with a FWHM of ~55 nm. These pulses are amplified by a 5.4 kHz Ti:sapphire regenerative amplifier. The output of the regenerative amplifier is split into two beams: the pump and the probe. The linearly polarized pump pulse induces birefringence in the sample by slightly aligning molecules along the electric field of the pulse. After the pump pulse, the induced birefringence is reduced as the molecules randomize their orientations. This process is tracked by the probe pulse which is polarized 45° relative to the pump. The probe beam is variably delayed by a delay line which allows the induced birefringence to be measured at many time points. For data past 15 ns, the mechanically delayed probe pulse is replaced with a 532 nm CW probe beam. The CW probing data are recorded with a 1 ns digitizer. This setup allows the orientational dynamics to be tracked from a few hundred femtoseconds out to the total randomization time of the molecules many decades of time later. Heterodyne detection is implemented in OHD-OKE experiments by making the probe pulse slightly elliptical. This results in a collinear local oscillator that amplifies the signal and allows for phase cycling.[57,58] Data are collected with a balanced detector and lock-in amplifier.

III. RESULTS AND DISCUSSION

A. OHD-OKE measurements on the bulk RTILs

OHD-OKE data were collected on the four neat ionic liquids. OHD-OKE is a nonresonant technique that uses ultrafast

TABLE I. Solvation dynamics parameters of C153 in bulk NTf$_2^-$ RTILs, the OHD-OKE decay time constants, and bulk viscosities.

Sample	τ_{s1} (ns)[a]	τ_{s2} (ns)[a]	τ_{s3} (ns)[a]	$\nu(\infty)$ (cm^{-1})[b]	τ_{OKE} (ns)[c]	η (cP)[d]
EmimNTf$_2$	...	0.10 ± 0.01	0.40 ± 0.03	$19\,250 \pm 24$	0.38 ± 0.01	36.3
BmimNTf$_2$	...	0.24 ± 0.02	1.11 ± 0.11	$19\,325 \pm 15$	1.16 ± 0.03	59.3
HmimNTf$_2$	0.11 ± 0.02	0.59 ± 0.03	2.15 ± 0.11	$19\,390 \pm 13$	2.08 ± 0.05	82.3
DmimNTf$_2$	0.16 ± 0.02	1.03 ± 0.06	4.45 ± 0.14	$19\,485 \pm 22$	4.63 ± 0.20	143.6

[a]Solvation decay constants.
[b]The final emission peak center frequency at equilibrium in the S$_1$ state.
[c]OHD-OKE decay constant.
[d]Bulk viscosities.

pulses of light to probe the orientational dynamics of bulk liquids. More specifically, OHD-OKE measures the anisotropic component of the time derivative of the second Legendre polynomial orientational correlation function.[59–61] Before discussing the results, it is important to discuss the source of the OHD-OKE signal. After short time (<2 ps), at which there may be collision-induced (interaction-induced) contributions to the signal, the signal is directly related to the anisotropic polarizability of the constituents of the liquid. This means that any asymmetric molecule or ion can contribute to the signal. For multicomponent liquids, like ionic liquids, more than one species can have anisotropic polarizability and contribute to the signal.

The ionic liquids studied here are composed of an NTf$_2^-$ anion and a cation consisting of an imidazolium ring and an alkyl chain of varying length. The structure of NTf$_2^-$ is asymmetric, so it will have anisotropic polarizability. However, theoretical calculations of the time derivative of the anisotropic polarizability of 1-alkyl-3-methylimidazoliumNTf$_2$ ionic liquids have shown that the NTf$_2^-$ anion contributes negligibly to the signal relative to the imidazolium moiety.[62] Thus, in these experiments, the OHD-OKE experiments are measuring the orientational relaxation dynamics of the cations. Given the size of the ions, the charge ordering in the local structure,[5,7] and the strong Columbic interactions among the ions, complete orientational relaxation of the cation cannot occur without total structural randomization of the liquid.

The OHD-OKE data for EmimNTf$_2$ are shown in Fig. 3 (green curve). The data span ~3 decades in time and ~4 decades in amplitude. The data for the other three liquids have the same functional form and the same data quality, but the dynamics are slower as the alkyl chain increases in length. The data consist of a power law at short time, < ~100 ps, followed by an exponential decay at long time. Here we are mainly interested in the final exponential decay time constant, which is the time for complete structural relaxation of the liquid. However, to properly obtain the exponential decay constant, it is useful to globally fit the entire curve.

The data were fit using the following equation:

$$F(t) = \frac{B}{2}\left(1 - erf\left(\frac{(\ln(t) - n)}{\sqrt{2}u}\right)\right)t^{-b}$$
$$+ \frac{C}{2}\left(1 + erf\left(\frac{\ln(t) - n}{\sqrt{2}u}\right)\right)e^{-t/\tau} + y_0. \quad (1)$$

This fitting function has been described thoroughly previously.[49] The general idea is rooted in schematic mode coupling
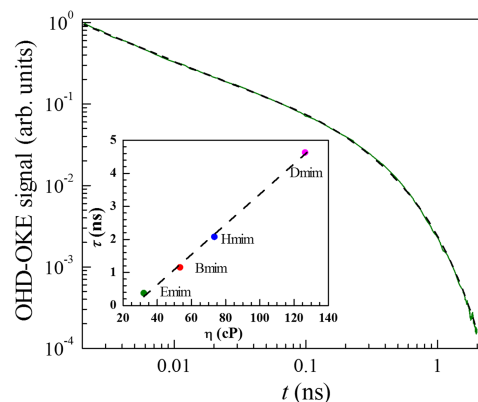

FIG. 3. OHD-OKE data for bulk EmimNTf$_2$ (green curve). The data span three decades in time and four decades in amplitude. The decay is a power law at short time (linear on the log plot) and exponential at long time. The dashed black curve is a fit to the data using Eq. (1). The inset shows a plot of the exponential decay constants for the four RTILs (colored circles) vs. viscosity and a linear fit to the points. The data fall on a line demonstrating that the relaxation is consistent with hydrodynamic theory. Viscosities were taken at 297.5 K to match the experimental temperature.

theory, which indicates that OHD-OKE data can be described by a series of up to three power law decays followed by an exponential decay.[63] Here we see a single power law, although we did not investigate very short times where the other power laws can appear. The power law reflects caged motions, while the final exponential decay is associated with complete orientational relaxation. The function in Eq. (1) describes the slowest von Schweidler power law (t^{-b})[63] and the final exponential decay [$\exp(-t/\tau)$]. More power law terms can be included in Eq. (1) to fit the very short time data. The transition of the power law to the exponential is reflected in the error functions, as the exponential is not present at short time and the power law is not present at long time. The crossover region between the power law and final exponential is determined by the parameters n and u, which give the time center and width of the transition from one functional form to the other.

In Fig. 3, the fit to EmimNTf$_2$ is shown as the black dashed curve. The fit is exceedingly good and provides an accurate determination of the parameters. The τ values for the four liquids and their viscosities are given in Table I as τ_{OKE}. The inset in Fig. 3 shows a plot of the τ values versus viscosity for the four liquids. The fact that the τ values for the four liquids fall on a line demonstrates that the orientational relaxation behaves as described by hydrodynamics. Hydrodynamic

theory predicts that the orientational relaxation should scale as the viscosity.

B. Bulk RTIL solvation dynamics

The bulk and confined RTIL responses to the $S_0 \rightarrow S_1$ excitation of C153 were observed by collecting the excited state population decay curves measured at the magic angle at emission wavelengths ranging from 460 nm to 580 nm in 2 nm increments. The observable in this study is the emission peak center as a function of time. Figure 4(a) shows a sample of the data taken on C153 in BmimNTf$_2$ from 100 ps to 1 ns. As time increases, the spectra shift to the red with the band shape remaining essentially constant. Figure 4(b) displays fluorescence decays on a semi-log plot at a number of wavelengths. On the blue side of the line, there is an initial fast decay as the spectrum shifts away from the observation wavelength. On the red side of line, there is an initial growth in fluorescence intensity as the spectrum shifts toward the observation wavelength. As can be seen in Fig. 4(b), at sufficiently long time, >2-3 ns, the decays are parallel lines, demonstrating that there is a single exponential fluorescence lifetime at all wavelengths.

These data were fit (red curves) with triexponential functions. The sign of the two fast components determines if they give rise to initial growth or decay. These fast components are caused by the time-dependent Stokes shift as quantified below. The fast component agreed with the time constants determined
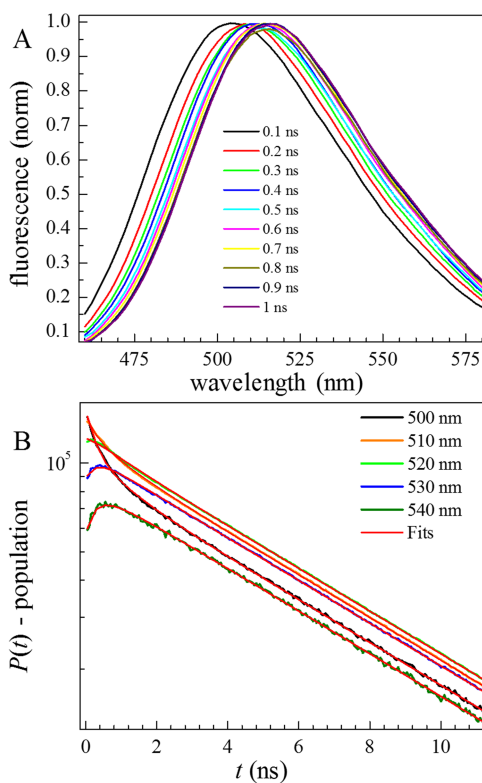

from the analysis of the Stokes shift. The slowest component is the fluorescence lifetime decay, and the fits yielded 6.0 ± 0.1 ns for all of the systems studied.

Because the band shape did not change substantially, each spectrum was fit with a Gaussian around the peak maximum (± 5 nm) to determine the peak position. The Gaussian function provided a good fit of the data over the limited range and was used only to determine the wavelength of the peak maximum. The peak maxima as a function of time were used to obtain spectral shift correlation functions (SSCFs),[64,65] $C(t)$, which are given by

$$C(t) = \frac{\nu(t) - \nu(\infty)}{\nu(0) - \nu(\infty)}, \qquad (2)$$

where $\nu(t)$, $\nu(0)$, and $\nu(\infty)$ represent the center of the emission peak at a given time t, $t = 0$, and $t = \infty$, respectively. $\nu(\infty)$ values are given in Table I. The SSCFs of the bulk ionic liquids are shown in Fig. 5 (solid colored curves). Because of the limitations imposed by the instrument response, the first fitted data point is at 100 ps. It should be noted that in many liquids a significant portion of the solvation dynamics occurs on shorter time scales, and other methods such as fluorescence upconversion or visible pump probe spectroscopy can be used to obtain very fast dynamics.[47,66] For the studies presented here, which extend to very long time, >15 ns, the time resolution is sufficient.

The data are not described well as single exponential decays. Data like these are frequently fit as multiexponential decays[42] and stretched exponential decays.[67] As discussed below, the data on the systems studied here are definitely multiexponential decays. The data were fit to the functional form

$$C_{Fit}(t) = \sum A_i e^{-t/\tau_i}. \qquad (3)$$

The fits to the bulk RTIL data are shown in Fig. 5 as the dashed black curves. The fit parameters are given in Table I. The EmimNTf$_2$ and BmimNTf$_2$ data were fit with biexponentials, while the HmimNTf$_2$ and DmimNTf$_2$ data were fit as triexponentials. Most likely the EmimNTf$_2$ and BmimNTf$_2$ data appear to be biexponentials because their fastest decay constant, τ_{s1}, is too fast to measure given the instrument response. Comparing EmimNTf$_2$ to HmimNTf$_2$, the τ_{s1} and τ_{s2} time constants for HmimNTf$_2$ are 110 ps and 590 ps, respectively. For EmimNTf$_2$, $\tau_{s2} = 100$ ps. If τ_{s1} is 5 or 6 times faster than τ_{s2} for EmimNTf$_2$ as it is for HmimNTf$_2$, then the EmimNTf$_2$

FIG. 4. (a) Fluorescence spectra of C153 for selected times ranging from 0.1 ns to 1 ns for BminNTf$_2$. As time increases, the spectrum shifts to the red side. The shape of the spectrum does not change. (b) Fluorescence decays for various detection wavelengths. At short time, on the blue side of the line, there is a fast decay as the spectrum shifts away from the wavelength. On the red side of the line, there is a short time buildup as the spectrum shifts toward the wavelength. At longer time, all of the decays are identical and single exponential (parallel lines).
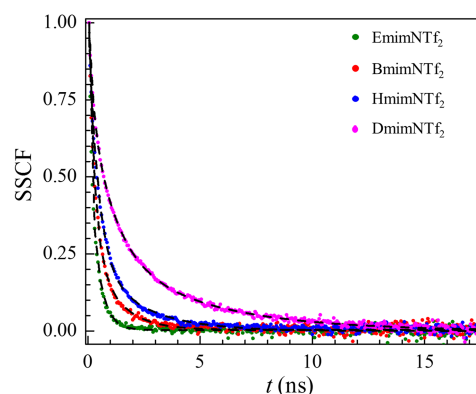

FIG. 5. C153 SSCF decays of the bulk RTIL samples (colored curves). The dashed black curves are multiexponential fits to the data.

fastest decay constant would be too fast to measure, which would also be true for BmimNTf$_2$. The solvation dynamics of C153 in BmimNTf$_2$ and EmimNTf$_2$ have been previously modeled as multiexponentials by Samanta and co-workers, and the current data are in good agreement with their results.[42] BmimNTf$_2$ was also studied by Maroncelli and co-workers. Their data are very similar to the BmimNTf$_2$ data presented here, but they fit the data with a stretched exponential.[68]

It can be seen in Table I that τ_{s3}, the slowest component of the time-dependent Stokes shift, and τ_{OKE} are identical for all four liquids within a small experimental error. τ_{OKE} are the time constants for complete structural randomization of the four liquids. The OHD-OKE experiment is a nonresonant measurement of the pure liquid and does not use an added probe. Therefore, the OHD-OKE measurements solely report on the bulk RTIL structural randomization. The fact that these two relaxation times are identical demonstrates that complete structural randomization is responsible for the slowest component of the solvation dynamics of each RTIL. This is an important result as it allows us to identify the origin of the slowest component of the solvation dynamics.

The match between τ_{s3} and τ_{OKE} for all four liquids is strong evidence that the multiexponential fit to the data in Fig. 5 is the proper description of the data. The data cannot be a stretched exponential if the slowest dynamics are single exponential decays in all four liquids. As an additional check on the appropriateness of assigning multiexponential functions to the decays, the data were also fit with stretched exponential functions, and the efficacy of the two fitting functions was tested with the Akaike Information Criterion (AIC) statistical test.[69] This test is commonly used to verify that the use of additional parameters increased the quality of the fits sufficiently for their use to be justified. The AIC test demonstrated that the quality of the multiexponential fit over the stretched exponential fit was overwhelmingly superior, justifying the use of extra parameters. Furthermore, lifetime density analysis (LDA)[70,71] was performed on each SSCF and on corresponding multiexponential fits and stretched exponential fits. The LDA is effectively a Laplace transform that provides the underlying spectral distribution. The LDA also clearly showed that the multiexponential fits were a far better representation of the data than stretched exponentials.

While the statistical tests confirm the validity of the multiexponential fits, the most important aspect of the fits is the agreement between the Stokes shift measurements and the OHD-OKE measurements. That these two fundamentally different types of experiments yield the same slowest exponential decays confirms the exponential nature of the Stokes shift decays and allows the slowest component of the Stokes shift data to be assigned to the complete structural randomization of the liquids.

C. RTIL solvation dynamics in SILM pores

PES 200 is a polyether sulfone membrane with an average pore size of ∼350 nm.[33,72] Previous 2D IR and polarization selective pump-probe studies of the CN stretch of SeCN$^-$ in EmimNTf$_2$ contained in mesoscopic pores of PES 200 showed that even in such large pores, the dynamics slowed substantially compared to the same experiments performed on the bulk
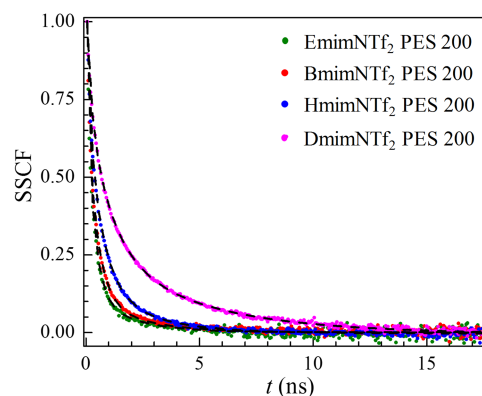

FIG. 6. C153 SSCF decays of the RTILs contained in the pores of PES 200 membranes with an average pore size of 350 nm (colored curves). The dashed black curves are multiexponential fits to the data.

liquid.[32,33] SeCN$^-$ experienced a factor of 3.6 increase in the decay time constant of the slowest component of the spectral diffusion.[33] These measurements demonstrated that a mesoscopically confined RTIL has different structural fluctuations, which implies a different structure, than the bulk RTIL in spite of the very large pore sizes. However, because of the limitations placed on the IR experiments by the vibrational lifetime, the experiments could only be conducted out to a time of several hundred picoseconds.

Like the bulk liquid samples discussed earlier, solvation dynamics of C153 in C$_n$mimNTf$_2$ RTILs were also measured while confined in the pores of PES 200 membranes. The data (colored curves) and the fits (black dashed curves) are shown in Fig. 6. The results of the multiexponential fits are given in Table II. The data taken on the RTILs in the membranes were all fit as triexponential decays. For EmimNTf$_2$ and BmimNTf$_2$, the decays have slowed compared to the bulk liquids enough that an initial fast component, which could not be observed in the bulk samples, was readily measured in the membrane samples. As can be seen by comparing the values in Tables I and II, confinement in the mesoscopic pores has a substantial impact on the solvation dynamics on the short chain RTILs that decreases as the chain length becomes longer.

First, consider the slowest components of the solvation dynamics, τ_{s3}, in the bulk (Table I) and in the membranes (Table II). For the bulk samples, comparison of the slowest component of the Stokes shift data to the final exponential decay of the OHD-OKE data (Table I) demonstrated that τ_{s3} is the time for complete structural randomization of the RTILs. It is reasonable to assume that the same is true for the RTILs in the membranes. The ratios of the membrane values to the bulk values are given in the column of Table II labeled τ_{s3} ratio. For EmimNTf$_2$, the ratio is 4.38. Thus, there is a very large slowing of the structural relaxation of the RTIL in the membrane. For BmimNTf$_2$, the ratio is 2.01, again a significant slowing but not nearly as substantial as in EmimNTf$_2$. For HmimNTf$_2$ and DmimNTf$_2$, the ratios are 1.13 and 1.03, respectively. The ratio for DmimNTf$_2$ is essentially 1 given the error bars on the measurements. Therefore, the membrane has a very large effect on the structural dynamics of EmimNTf$_2$ but basically no effect for DmimNTf$_2$. Comparison of τ_{s2} for the bulk RTILs

TABLE II. Solvation dynamics of C153 in NTf_2^- RTILs confined within PES 200 membranes.

Sample	τ_{s1} (ns)[a]	τ_{s2} (ns)[a]	τ_{s3} (ns)[a]	τ_{s2} ratio[b]	τ_{s3} ratio[b]	$\nu(\infty)$ (cm^{-1})[c]	η_{eff} (cP)[d]
EmimNTf$_2$	0.07 ± 0.03	0.33 ± 0.05	1.77 ± 0.34	3.38	4.38	19 305 ± 14	174
BmimNTf$_2$	0.09 ± 0.02	0.46 ± 0.05	2.23 ± 0.29	1.88	2.01	19 315 ± 21	119
HmimNTf$_2$	0.14 ± 0.02	0.67 ± 0.06	2.53 ± 0.27	1.13	1.17	19 390 ± 22	96
DmimNTf$_2$	0.19 ± 0.02	1.04 ± 0.08	4.60 ± 0.23	1.00	1.03	19 475 ± 18	148

[a]Solvation time constants.
[b]Solvation time constant ratios (confined:bulk).
[c]The final emission peak center frequency at equilibrium in the S_1 state.
[d]The effective viscosity of RTILs in the pores; the bulk viscosity multiplied by the τ_{s3} ratio. See Table I for bulk viscosities.

and the RTILs in the membrane shows the same basic trend as found for the slowest structural relaxation component. The ratios of the membrane bound RTIL to the bulk RTIL given in Table II as the τ_{s2} ratio show a large slowing for EmimNTf$_2$ and BmimNTf$_2$ and much less change for HmimNTf$_2$ and no change for DmimNTf$_2$. It is interesting to note that the τ_{s2} ratio for EmimNTf$_2$ is essentially the same and the time scale of the relaxation is very similar to the values measured with 2D IR spectroscopy on the vibrational probe SeCN$^-$.[33]

The 2D IR experiments on SeCN$^-$[33] and CO$_2$[32] in EmimNTf$_2$ in PES 200 membranes both showed substantial slowing of the RTIL's structural dynamics compared to the bulk RTIL. However, the slowest dynamics observed in these experiments in both the bulk and membrane bound RTILs were on the order of a few 100 ps in contrast to the much slower dynamics observed with the Stokes shift measurements. For the vibrational probes used in 2D IR experiments, only those degrees of freedom of the medium that contribute to the inhomogeneously broadened absorption line will be observed in the measurement of the structural dynamics. A 2D IR comparison study in which bulk RTIL dynamics were measured using SeCN$^-$, a small probe anion, and a vibrational probe that was part of the imidazolium cation showed that the cation probe picked up much slower time scale dynamics consistent with OHD-OKE measurements of the complete randomization of the liquid.[21] Here, the Stokes shift measurements on C153 observed the slowest time scale dynamics as well as faster dynamics because C153 is strongly coupled to the RTIL structural degrees of freedom. Strong coupling of C153 to the RTILs is discussed in connection with the C153 orientational relaxation measurement presented in the supplementary material. However, the 2D IR experiments were able to observe very fast structural dynamics that were too fast to observe given the time resolution of the TCSPC experimental method used here.

Through comparison to the OHD-OKE data, we have identified the slowest component of the time-dependent Stokes shift as the time for complete structural randomization of the RTILs. It is not immediately obvious what gives rise to the faster time scale dynamics. Simulations by Terranova and Corcelli suggest that these dynamics may be linked to translational motions of the anions.[47] In addition, a shift of 55 cm^{-1} (~1.5 nm) in the $\nu(\infty)$ value in EmimNTf$_2$ upon confinement was observed (see Tables I and II). Within the experimental error, the values of $\nu(\infty)$ are the same in the bulk RTILs and the RTILs in the membranes for the three longer chain RTILs. The shift seen in $\nu(\infty)$ for EmimNTf$_2$ is another observable

that shows that confinement has the largest influence on the structure of the shortest chain length RTIL.

The OHD-OKE measurements of the complete structural relaxation of the bulk RTILs and the slowest components of the Stokes shift data were identical within the error (compare columns 4 and 6 of Table I). In addition, the OHD-OKE data displayed hydrodynamic behavior, that is, the plot of the relaxation times vs. the viscosity fall on a line (see the inset of Fig. 3). Then effective viscosities of the RTILs in the membranes can be obtained from the bulk RTIL viscosities (given in Table I) by multiplying by the τ_{s3} ratios. The effective viscosities, η_{eff}, in cP are given in the last column of Table II. For EmimNTf$_2$ through DmimNTf$_2$, the values are 174, 119, 96, and 148. This is a remarkable result, although it is based on the assumption that the slowest component of the RTIL relaxation in the membrane is equivalent to the slowest component in the bulk. Given this assumption, the results show that the viscosity is lower in HmimNTf$_2$ than in EmimNTf$_2$ or BmimNTf$_2$ in the membrane. This result arises because the membrane has a large influence on the structural dynamics for the short chain RTILs but little or no effect on the long chain RTILs. This result has important implications for the use of SILMs for CO$_2$ capture.[4,29,32,33] In the CO$_2$ capture application, CO$_2$ enters the membrane and dissolves in the RTIL on one side where the CO$_2$ concentration is high, and then diffuses through the pores, to the other side, where it emerges and is collected.[30,73] The effective viscosities indicate that HmimNTf$_2$ might be a better RTIL in the membrane in this application because of faster diffusion than EmimNTf$_2$ in spite of the fact that the EmimNTf$_2$ viscosity is much lower in the bulk liquid. However, it is important to note that in a CO$_2$ capture application, the membrane will be exposed to water vapor, and the RTIL will be saturated with a small amount of water. Water lowers the RTIL viscosity, and EmimNTf$_2$ contains more water at saturation than HmimNTf$_2$. Thus, determining the effective viscosities for the water saturated RTILs in the membranes would be useful. Several factors, such as the CO$_2$ solubility in the membrane bound RTILs, also need to be taken into account when selecting the best SILM solvent.

The results presented earlier demonstrate that the interactions of the short chain length RTILs interacting with the polyether sulfone pore interface can have a very long range influence on the RTIL dynamics, >100 nm, and by implication, on the structure of the mesoscopically confined RTILs. However, as the chain length becomes long, the effect is reduced and is absent for the 10 carbon chain RTILs, DmimNTf$_2$. A variety of experiments have indicated that the RTIL structure

near an interface differs substantially from the bulk structure, but these experiments examined much shorter distances than those investigated here. Simulations by Margulis and co-workers indicate that long chained RTILs form lamellar structures at the liquid-vacuum interface persisting for several nanometers.[74] While a vacuum interface is very different from the polymer interface of the pores studied here, the simulation results may not be inconsistent with the bulk-like behavior of DmimNTf$_2$ in the pores. If a lamellar structure extended 5 nm from the interface, and as a simple approximation taking the pores to be cylinders, the 5 nm interfacial region would only comprise ~5% of the pore volume. This percentage would likely not be enough to observe an effect on the measured dynamics. In addition, the planar vacuum interface may have more effect on the long chain RTIL structure than the non-planar, more disordered polymer pore wall.

The membranes' large influence on the dynamics of the shortest chain length RTIL and the decreased influence as the chain length grows, with no effect on the longest chain length, can be caused by the differences in the polar-apolar structure of the RTILs. Theoretical calculations show that the positive charge on imidazolium cations is delocalized over the ring as well as the first two carbon atoms on the alkyl chain.[8] Therefore, Emim$^+$ does not have an apolar portion of the cation and is ionic throughout the liquid. The liquid is a collection of cations and anions resulting in extensive charge ordering. The last two carbons in the chain in Bmim$^+$ will not carry positive charge and will behave as regular hydrocarbons. Simulations show that although BmimNTf$_2$ has apolar regions, they are local and not mesoscopically extended.[6–8] HmimNTf$_2$ is the first RTIL in the series that maintains extended apolar regions.[6–8] The apolar regions are merged into non-local domains that percolate through the RTIL. The size of these apolar domains grows with the chain length.

The structures of all of the RTILs are undoubtedly different at the PES interface than they are in the bulk liquid. The oxygen on the sulfone moieties will carry a partial negative charge. Therefore, it is likely that cations will preferentially be present at the interface. The preferential arrangement of interfacial cations will lead to a non-bulk arrangement of anions. For EmimNTf$_2$, this non-bulk cation-anion organization may propagate out from the interface, creating a non-bulk structure of large distances greater than 100 nm. This non-bulk structure produces the non-bulk dynamics in the membrane pores. The long range non-bulk like charge ordering induced by the PES interface occurring for EmimNTf$_2$ has competition in BmimNTf$_2$ from the tendency for the alkyl chains to aggregate as they do to some extent in the bulk liquid. The alkyl-alkyl interactions somewhat mitigate the modified charge ordering induced by the interface, but the effect of the interface is still substantial. Starting with HmimNTf$_2$, there is a strong driving force to establish extended apolar domains. The Stokes shift data show that the structural dynamics of HmimNTf$_2$ are close to bulk, indicating that most of the RTIL in the pores is close to bulk. With DmimNTf$_2$, the driving force to form the very extensive large apolar regions overcomes the charge ordering at and near the interface, resulting in the vast majority of the RTILs in the pores to have the bulk liquid structure and therefore bulk liquid dynamics.

Undoubtedly, all of the liquids have perturbed structures at the interfaces. Competition between altered charge ordering induced by the interface and the drive to form apolar domains away from the interface determines the extent to which the entire liquid restructures. This explanation is consistent with the experiment and simulations that observe the modified RTIL structure within a few nanometers of an interface.[74] Longer chain RTILs behave in a manner that is akin to water in reverse micelles. For large reverse micelles, the water structure is modified by the interface, but the driving force to form the normal essentially tetrahedral hydrogen bond network overcomes the structural modification of the hydrogen bond geometry induced by the interface within a few nanometers of the interface.[34] However, for EmimNTf$_2$, and to some extent BmimNTf$_2$, the tendency to form extended apolar regions is absent. It is the formation of extended apolar regions in the longer alkyl chain length RTILs which is responsible for relaxing the modified structure induced by the interface back to the bulk structure as the distance from the interfaces becomes large.

IV. CONCLUDING REMARKS

Solvation dynamics were measured by observing the time-dependent fluorescence Stokes shift of C153 in a series of ionic liquids, EmimNTf$_2$, BmimNTf$_2$, HmimNTf$_2$, and DmimNTf$_2$, in both the bulk RTILs and in the RTILs confined in the pores of PES 200 membranes. The average pore size in the membranes is ~350 nm.[33,72] In all four liquids, the Stokes shift correlation function decayed as a multiexponential function. In the bulk liquids, the slowest component of the SSCF decays perfectly matched the exponential decay times for complete structural randomization of the pure liquids using optical heterodyne-detected optical Kerr effect experiments, which do not require adding a probe molecule. The agreement between the two types of measurements demonstrates that the slowest component of the Stokes shift dynamics is caused by the structural randomization of the RTILs.

The Stokes shift measurements on C153 in EmimNTf$_2$ in the pores show a substantial slowing of the RTIL's structural dynamics in spite of the very large size of the pores. The time for complete structural randomization of EmimNTf$_2$ in the pores is ~4.4 times slower than in the bulk RTIL. This result is consistent with previous 2D IR experiments that could observe the faster time scale dynamics of bulk and membrane bound EmimNTf$_2$ but not the full range of dynamical time scales.[32,33] While all liquids' structures and dynamics will be affected by interaction with an interface, the influence of the interface generally dissipates within a few nanometers. For EmimNTf$_2$, the influence of the interface changes the structure and dynamics for distances on the order of 100 nm. The slowing with BmimNTf$_2$ in the pores was ~2, and by HmimNTf$_2$, the slowing was small, 1.13. For the longest chain length studied, DmimNTf$_2$, the structural dynamics in the pores were indistinguishable for those of the bulk liquid. The dynamics and structure of the RTIL are intimately related. The dynamics change because the structure is different. Thus, the membrane has a long distance scale effect on the liquid structure of

EmimNTf$_2$ but no long range influence on the structure of DmimNTf$_2$.

To understand the large change induced by confinement in the pores of EmimNTf$_2$ but the decreasing influence of the pores as the alkyl chain length increases, we proposed a model that involves a competition between the interaction with the interface, which will change the RTIL structure over some distance scale, and the impetus for the RTIL to form distinct ionic and apolar regions. Because the positive charge of the imidazolium cation is delocalized over the first two carbons of an alkyl chain,[8] EmimNTf$_2$ is a collection of cations and anions with no apolar moieties. The interface establishes a non-bulk structure that presumably changes the cation-anion charge ordering arrangement. Once established, this non-bulk structure propagates out from the interface for a long distance, producing the observed large change in the solvation dynamics. Bmim$^+$ has two nonpolar carbons, which is not long enough to form extended apolar regions.[6–8] However, there will be competition to some degree between maintaining the non-bulk charge ordering established by the interface and the tendency for the alkyl portions of the butyl chains to aggregate. The non-bulk dynamics are greatly reduced but still prominent. For HmimNTf$_2$, there is a strong driving force to form extended apolar regions that are characteristic of the bulk structure. The formation of the apolar regions almost negates the influence of the interface over long distances, and the observed dynamics are almost the same as in the bulk RTIL. With the long alkyl chains of DmimNTf$_2$, the formation of apolar regions wins out over interface induced structuring, and the dynamics of the RTIL in membrane pores are indistinguishable from those of the bulk liquid.

The model of the relationship between the long range structural perturbation by the interface and the alkyl chain length is consistent with previous measurements and simulations that observed differences from the bulk structure at distances of a few nanometers from the interface. It will be interesting and important to look at interfaces other than those in PES membranes. The results presented here provide insights for the use of SILMs in CO$_2$ capture and other applications as they show that the properties of the bulk liquid can be substantially modified even in the relatively large pores of PES membranes.

SUPPLEMENTARY MATERIAL

See supplementary material for experiments and analysis of the rotational dynamics C153 probe in the bulk RTIL samples.

ACKNOWLEDGMENTS

[1] Y. Paulechka, D. H. Zaitsau, G. Kabo, and A. Strechan, "Vapor pressure and thermal stability of ionic liquid 1-butyl-3-methylimidazolium bis (trifluoromethylsulfonyl) amide," Thermochim. Acta **439**(1), 158–160 (2005).

[2] R.-S. Kühnel, N. Böckenfeld, S. Passerini, M. Winter, and A. Balducci, "Mixtures of ionic liquid and organic carbonate as electrolyte with improved safety and performance for rechargeable lithium batteries," Electrochim. Acta **56**(11), 4092–4099 (2011).

[3] M. Kosmulski, J. Gustafsson, and J. B. Rosenholm, "Thermal stability of low temperature ionic liquids revisited," Thermochim. Acta **412**(1), 47–53 (2004).

[4] M. Ramdin, T. W. de Loos, and T. J. H. Vlugt, "State-of-the-art of CO$_2$ capture with ionic liquids," Ind. Eng. Chem. Res. **51**(24), 8149–8177 (2012).

[5] R. Hayes, G. G. Warr, and R. Atkin, "Structure and nanostructure in ionic liquids," Chem. Rev. **115**(13), 6357–6426 (2015).

[6] Y. Wang and G. A. Voth, "Unique spatial heterogeneity in ionic liquids," J. Am. Chem. Soc. **127**(35), 12192–12193 (2005).

[7] J. N. Canongia Lopes and A. A. Padua, "Nanostructural organization in ionic liquids," J. Phys. Chem. B **110**(7), 3330–3335 (2006).

[8] S. M. Urahata and M. C. Ribeiro, "Structure of ionic liquids of 1-alkyl-3-methylimidazolium cations: A systematic computer simulation study," J. Chem. Phys. **120**(4), 1855–1863 (2004).

[9] O. Russina, A. Triolo, L. Gontrani, R. Caminiti, D. Xiao, L. G. Hines, R. A. Bartsch, E. L. Quitevis, N. V. Plechkova, and K. R. Seddon, "Morphology and intermolecular dynamics of 1-alkyl-3-methylimidazolium bis{(trifluoromethane)sulfonyl}amide ionic liquids: Structural and dynamic evidence of nanoscale segregation," J. Phys.: Condens. Matter **21**(42), 424121 (2009).

[10] A. Triolo, O. Russina, H.-J. Bleif, and E. Di Cola, "Nanoscale segregation in room temperature ionic liquids," J. Phys. Chem. B **111**(18), 4641–4644 (2007).

[11] M. Mizoshiri, T. Nagao, Y. Mizoguchi, and M. Yao, "Dielectric permittivity of room temperature ionic liquids: A relation to the polar and nonpolar domain structures," J. Chem. Phys. **132**(16), 164510 (2010).

[12] D. A. Turton, J. Hunger, A. Stoppa, G. Hefter, A. Thoman, M. Walther, R. Buchner, and K. Wynne, "Dynamics of imidazolium ionic liquids from a combined dielectric relaxation and optical Kerr effect study: Evidence for mesoscopic aggregation," J. Am. Chem. Soc. **131**(31), 11140–11146 (2009).

[13] M. Imanari, K. I. Uchida, K. Miyano, H. Seki, and K. Nishikawa, "NMR study on relationships between reorientational dynamics and phase behaviour of room-temperature ionic liquids: 1-alkyl-3-methylimidazolium cations," Phys. Chem. Chem. Phys. **12**(12), 2959–2967 (2010).

[14] C. Chiappe, "Nanostructural organization of ionic liquids: Theoretical and experimental evidences of the presence of well defined local structures in ionic liquids," Montash. Chem. - Chem. Mon. **138**(11), 1035–1043 (2007).

[15] S. Mandal, S. Ghosh, C. Banerjee, J. Kuchlyan, D. Banik, and N. Sarkar, "A novel ionic liquid-in-oil microemulsion composed of biologically acceptable components: An excitation wavelength dependent fluorescence resonance energy transfer study," J. Phys. Chem. B **117**(11), 3221–3231 (2013).

[16] K. Fruchey, C. M. Lawler, and M. Fayer, "Investigation of nanostructure in room temperature ionic liquids using electronic excitation transfer," J. Phys. Chem. B **116**(10), 3054–3064 (2012).

[17] J. Guo, G. A. Baker, P. C. Hillesheim, S. Dai, R. W. Shaw, and S. M. Mahurin, "Fluorescence correlation spectroscopy evidence for structural heterogeneity in ionic liquids," Phys. Chem. Chem. Phys. **13**(27), 12395–12398 (2011).

[18] D. Xiao, J. R. Rajian, S. Li, R. A. Bartsch, and E. L. Quitevis, "Additivity in the optical Kerr effect spectra of binary ionic liquid mixtures: Implications for nanostructural organization," J. Phys. Chem. B **110**(33), 16174–16178 (2006).

[19] D. Xiao, J. R. Rajian, A. Cady, S. Li, R. A. Bartsch, and E. L. Quitevis, "Nanostructural organization and anion effects on the temperature

dependence of the optical Kerr effect spectra of ionic liquids," J. Phys. Chem. B **111**(18), 4669–4677 (2007).

[20] A. L. Sturlaugson, K. S. Fruchey, and M. D. Fayer, "Orientational dynamics of room temperature ionic liquid/water mixtures: Water-induced structure," J. Phys. Chem. B **116**(6), 1777–1787 (2012).

[21] S. A. Yamada, H. E. Bailey, A. Tamimi, C. Li, and M. D. Fayer, "Dynamics in a room-temperature ionic liquid from the cation perspective: 2D IR vibrational echo spectroscopy," J. Am. Chem. Soc. **139**(6), 2408–2420 (2017).

[22] Z. Ren, A. S. Ivanova, D. Couchot-Vore, and S. Garrett-Roe, "Ultrafast structure and dynamics in ionic liquids: 2D-IR spectroscopy probes the molecular origin of viscosity," J. Phys. Chem. Lett. **5**(9), 1541–1546 (2014).

[23] K. Shimizu, C. E. Bernardes, and J. N. Canongia Lopes, "Structure and aggregation in the 1-alkyl-3-methylimidazolium bis (trifluoromethylsulfonyl) imide ionic liquid homologous series," J. Phys. Chem. B **118**(2), 567–576 (2014).

[24] M. A. Rocha, C. F. Lima, L. R. Gomes, B. Schroäder, J. A. Coutinho, I. M. Marrucho, J. M. Esperança, L. P. Rebelo, K. Shimizu, and J. N. C. Lopes, "High-accuracy vapor pressure data of the extended [$C_nC_1$im][Ntf$_2$] ionic liquid series: Trend changes and structural shifts," J. Phys. Chem. B **115**(37), 10919–10926 (2011).

[25] M. A. Rocha, C. M. Neves, M. G. Freire, O. Russina, A. Triolo, J. A. Coutinho, and L. M. Santos, "Alkylimidazolium based ionic liquids: Impact of cation symmetry on their nanoscale structural organization," J. Phys. Chem. B **117**(37), 10889–10897 (2013).

[26] P. Scovazzo, A. E. Visser, J. H. Davis, R. D. Rogers, C. A. Koval, D. L. DuBois, and R. D. Noble, *Ionic Liquids* (American Chemical Society, 2002), Vol. 818, pp. 69–87.

[27] A. J. Kemperman, D. Bargeman, T. Van Den Boomgaard, and H. Strathmann, "Stability of supported liquid membranes: State of the art," Sep. Sci. Technol. **31**(20), 2733–2762 (1996).

[28] X. Zhang, X. Zhang, H. Dong, Z. Zhao, S. Zhang, and Y. Huang, "Carbon capture with ionic liquids: Overview and progress," Energy Environ. Sci. **5**(5), 6668–6681 (2012).

[29] J. F. Brennecke and B. E. Gurkan, "Ionic liquids for CO_2 capture and emission reduction," J. Phys. Chem. Lett. **1**(24), 3459–3464 (2010).

[30] C. Myers, H. Pennline, D. Luebke, J. Ilconich, J. K. Dixon, E. J. Maginn, and J. F. Brennecke, "High temperature separation of carbon dioxide/hydrogen mixtures using facilitated supported ionic liquid membranes," J. Membr. Sci. **322**(1), 28–31 (2008).

[31] L. Lozano, C. Godinez, A. De Los Rios, F. Hernández-Fernández, S. Sánchez-Segado, and F. J. Alguacil, "Recent advances in supported ionic liquid membrane technology," J. Membr. Sci. **376**(1), 1–14 (2011).

[32] J. Y. Shin, S. A. Yamada, and M. D. Fayer, "Carbon dioxide in a supported ionic liquid membrane: Structural and rotational dynamics measured with 2D IR and pump-probe experiments," J. Am. Chem. Soc. **139**(32), 11222 (2017).

[33] J. Y. Shin, S. A. Yamada, and M. D. Fayer, "Dynamics of a room temperature ionic liquid in supported ionic liquid membranes vs the bulk liquid: 2D IR and polarized IR pump–probe experiments," J. Am. Chem. Soc. **139**(1), 311–323 (2016).

[34] D. E. Moilanen, E. E. Fenn, D. Wong, and M. D. Fayer, "Water dynamics in large and small reverse micelles: From two ensembles to collective behavior," J. Chem. Phys. **131**(1), 014704 (2009).

[35] P. K. Mandal, S. Saha, R. Karmakar, and A. Samanta, "Solvation dynamics in room temperature ionic liquids: Dynamic Stokes shift studies of fluorescence of dipolar molecules," Curr. Sci. **90**(3), 301–310 (2006).

[36] E. W. Castner, Jr., M. Maroncelli, and G. R. Fleming, "Subpicosecond resolution studies of solvation dynamics in polar aprotic and alcohol solvents," J. Chem. Phys. **86**(3), 1090–1097 (1987).

[37] W. Jarzeba, G. C. Walker, A. E. Johnson, and P. F. Barbara, "Nonexponential solvation dynamics of simple liquids and mixtures," Chem. Phys. **152**(1-2), 57–68 (1991).

[38] Š. Vajda, R. Jimenez, S. J. Rosenthal, V. Fidler, G. R. Fleming, and E. W. Castner, "Femtosecond to nanosecond solvation dynamics in pure water and inside the Γ-cyclodextrin cavity," J. Chem. Soc., Faraday Trans. **91**(5), 867–873 (1995).

[39] L. Onsager, "Reciprocal relations in irreversible processes. II," Phys. Rev. **38**(12), 2265 (1931).

[40] A. Samanta, "Dynamic Stokes shift and excitation wavelength dependent fluorescence of dipolar molecules in room temperature ionic liquids," J. Phys. Chem. B **110**(28), 13704–13716 (2006).

[41] T. Fonseca and B. M. Ladanyi, "Breakdown of linear response for solvation dynamics in methanol," J. Phys. Chem. **95**(6), 2116–2119 (1991).

[42] R. Karmakar and A. Samanta, "Dynamics of solvation of the fluorescent state of some electron donor–acceptor molecules in room temperature ionic liquids, [bmim][(CF_3SO_2)$_2$N] and [Emim] [(CF_3SO_2)$_2$N]," J. Phys. Chem. A **107**, 7340–7346 (2003).

[43] S. Arzhantsev, N. Ito, M. Heitz, and M. Maroncelli, "Solvation dynamics of coumarin 153 in several classes of ionic liquids: Cation dependence of the ultrafast component," Chem. Phys. Lett. **381**(3), 278–286 (2003).

[44] B. Lang, G. Angulo, and E. Vauthey, "Ultrafast solvation dynamics of coumarin 153 in imidazolium-based ionic liquids," J. Phys. Chem. A **110**(22), 7028–7034 (2006).

[45] T. Shimomura, T. Takamuku, and T. Yamaguchi, "Clusters of imidazolium-based ionic liquid in benzene solutions," J. Phys. Chem. B **115**(26), 8518–8527 (2011).

[46] D. Xiao, L. G. Hines, Jr., R. A. Bartsch, and E. L. Quitevis, "Intermolecular vibrational motions of solute molecules confined in nonpolar domains of ionic liquids," J. Phys. Chem. B **113**(14), 4544–4548 (2009).

[47] Z. Terranova and S. Corcelli, "On the mechanism of solvation dynamics in imidazolium-based ionic liquids," J. Phys. Chem. B **117**(49), 15659–15666 (2013).

[48] A. L. Sturlaugson, A. Y. Arima, H. E. Bailey, and M. D. Fayer, "Orientational dynamics in a lyotropic room temperature ionic liquid," J. Phys. Chem. B **117**, 14775–14784 (2013).

[49] H. E. Bailey, Y.-L. Wang, and M. D. Fayer, "The impact of hydrogen bonding on the dynamics and structure of protic ionic liquid/water binary mixtures," J. Phys. Chem. B **121**(36), 8564–8576 (2017).

[50] K. P. Sokolowsky, H. E. Bailey, and M. D. Fayer, "New divergent dynamics in the isotropic to nematic phase transition of liquid crystals measured with 2D IR vibrational echo spectroscopy," J. Chem. Phys. **141**(19), 194502 (2014).

[51] K. P. Sokolowsky, H. E. Bailey, and M. D. Fayer, "Length scales and structural dynamics in nematogen pseudonematic domains measured with 2D IR vibrational echoes and optical Kerr effect experiments," J. Phys. Chem. B **118**, 7856–7868 (2014).

[52] H. Cang, V. N. Novikov, and M. D. Fayer, "Logarithmic decay of the orientational correlation function in supercooled liquids on the ps to ns time scale," J. Chem. Phys. **118**(6), 2800–2807 (2003).

[53] H. Cang, V. Novikov, and M. Fayer, "Experimental observation of a nearly logarithmic decay of the orientational correlation function in supercooled liquids on the picosecond-to-nanosecond time scales," Phys. Rev. Lett. **90**(19), 197401 (2003).

[54] J. A. Widegren, A. Laesecke, and J. W. Magee, "The effect of dissolved water on the viscosities of hydrophobic room-temperature ionic liquids," Chem. Commun. **2005**(12), 1610–1612.

[55] M. J. Earle, C. M. Gordon, N. V. Plechkova, K. R. Seddon, and T. Welton, "Decolorization of ionic liquids for spectroscopy," Anal. Chem. **79**(2), 758–764 (2007).

[56] P. Wirth, S. Schneider, and F. Dörr, "S$_1$-lifetimes of triphenylmethane and indigo dyes determined by the two-photon-fluorescence technique," Opt. Commun. **20**(1), 155–158 (1977).

[57] S. Kinoshita, Y. Sakai, J. Miyazaki, and J. Watanabe, "Fundamental aspects of light scattering and optical Kerr effect spectroscopy," Eur. Phys. J.: Spec. Top. **209**, 1–100 (2012).

[58] N. A. Smith and S. R. Meech, "Optically-heterodyne-detected optical Kerr effect (OHD-OKE): Applications in condensed phase dynamics," Int. Rev. Phys. Chem. **21**, 75–100 (2002).

[59] F. W. Deeg, J. J. Stankus, S. R. Greenfield, V. J. Newell, and M. D. Fayer, "Anisotropic reorientational relaxation of biphenyl: Transient grating optical Kerr effect measurements," J. Chem. Phys. **90**, 6893 (1989).

[60] S. Ruhman, L. R. Williams, A. G. Joly, B. Kohler, and K. A. Nelson, "Nonrelaxational inertial motion in Cs$_2$ liquid observed by time-resolved impulsive stimulated scattering," J. Phys. Chem. **91**, 2237–2240 (1987).

[61] Y. X. Yan and K. A. Nelson, "Impulsive stimulated light scattering. I. General theory," J. Chem. Phys. **87**(11), 6240–6256 (1987).

[62] G. Giraud, C. M. Gordon, I. R. Dunkin, and K. Wynne, "The effects of anion and cation substitution on the ultrafast solvent dynamics of ionic liquids: A time-resolved optical Kerr-effect spectroscopic study," J. Chem. Phys. **119**(1), 464–477 (2003).

[63] W. Götze and L. Sjögren, "The mode coupling theory of structural relaxations," Transp. Theory Stat. Phys. **24**(6-8), 801–853 (1995).

[64] E. Bart, A. Meltsin, and D. Huppert, "Excited-state solvation dynamics in solid tetraalkylammonium salts," J. Phys. Chem. **99**(22), 9253–9257 (1995).

[65] E. Bart, A. Meltsin, and D. Huppert, "Solvation dynamics of coumarin 153 in molten salts," J. Phys. Chem. **98**(13), 3295–3299 (1994).

[66]M. Horng, J. Gardecki, A. Papazyan, and M. Maroncelli, "Subpicosecond measurements of polar solvation dynamics: Coumarin 153 revisited," J. Phys. Chem. **99**(48), 17311–17337 (1995).

[67]H. Jin, X. Li, and M. Maroncelli, "Heterogeneous solute dynamics in room temperature ionic liquids," J. Phys. Chem. B **111**(48), 13473–13478 (2007).

[68]H. Jin, G. A. Baker, S. Arzhantsev, J. Dong, and M. Maroncelli, "Solvation and rotational dynamics of coumarin 153 in ionic liquids: Comparisons to conventional solvents," J. Phys. Chem. B **111**(25), 7291–7302 (2007).

[69]H. Bozdogan, "Model selection and akaike's information criterion (AIC): The general theory and its analytical extensions," Psychometrika **52**(3), 345–370 (1987).

[70]C. Slavov, H. Hartmann, and J. Wachtveitl, "Implementation and evaluation of data analysis strategies for time-resolved optical spectroscopy," Anal. Chem. **87**(4), 2328–2336 (2015).

[71]M. A. Berg and H. Kaur, "Nonparametric analysis of nonexponential and multidimensional kinetics. I. Quantifying rate dispersion, rate heterogeneity, and exchange dynamics," J. Chem. Phys. **146**(5), 054104 (2017).

[72]S. Ramakrishnan, C. McDonald, R. Prud'homme, and J. Carbeck, "Latex composite membranes: Structure and properties of the discriminating layer," J. Membr. Sci. **231**, 57–70 (2004).

[73]S. Hanioka, T. Maruyama, T. Sotani, M. Teramoto, H. Matsuyama, K. Nakashima, M. Hanaki, F. Kubota, and M. Goto, "CO_2 separation facilitated by task-specific ionic liquids using a supported liquid membrane," J. Membr. Sci. **314**(1), 1–4 (2008).

[74]W. D. Amith, J. J. Hettige, E. W. Castner, Jr., and C. J. Margulis, "Structures of ionic liquids having both anionic and cationic octyl tails: Lamellar vacuum interface vs sponge-like bulk order," J. Phys. Chem. Lett. **7**(19), 3785–3790 (2016).